Ref: Aşıkoğlu A, Avşar Ö, Lourenço PB, Silva LC (2019) Effectiveness of seismic retrofitting of a historical masonry structure: Kütahya Kurşunlu Mosque, Turkey. Bull Earthq Eng. doi: 10.1007/s10518-019-00603-6

Effectiveness of Seismic Retrofitting of a Historical Masonry Structure: Kütahya Kurşunlu Mosque, Turkey

Abide Aşıkoğlu[1*], Özgür Avşar[2], Paulo B. Lourenço[1], Luís C. Silva[1]

Abstract A seismic performance assessment of historical Kütahya Kurşunlu Mosque in Turkey is presented before and after it has been retrofitted. Site investigations were carried out to identify structural conditions, in which severe cracks, especially on the dome, were mapped. Regarding damage conditions, the Mosque has undergone several interventions, including retrofitting actions, in order to improve its seismic performance and global structural behavior. Effectiveness of seismic retrofitting of the Mosque was investigated by using the finite element method. Two representative structural models of the Mosque, namely non-retrofitted and retrofitted, were generated as a three-dimensional finite element model using an advanced structural analysis software. Ambient vibration measurements were performed to identify modal properties of the Mosque. Thus, the finite element model was calibrated and improved according to the experimental modal data. Nonlinear pushover and dynamic analyses were conducted to evaluate the seismic performance of the historical Mosque. This paper aims to demonstrate the effectiveness of the adopted retrofitting by comparing the models (before and after retrofitting) and, also, to validate the nonlinear behavior of the model by comparing it with the existing damage on the Mosque.

Keywords: Historical masonry mosque, Finite element analysis, Nonlinear analysis, Seismic performance, Retrofitting.

1 Introduction

Cultural heritage buildings are physical manifestations of the history and material evidence of past generations, craftsmanship, techniques, and cultural context (Orbaşlı, 2007). Thus, conservation of the built heritage plays an important role to maintain and promote national identity and cultural diversity within—and also between—the communities. In this sense, conservation of historical structures should be conducted according to the principle of minimum intervention, as admitted in ICOMOS (2013). Each ancient structure has unique architectural, material, and structural properties. As addressed in Roca (2006), these structures have complex geometries and diverse materials, and they suffered changes due to long-term effects, imposed damage, or repair works. Structural engineering applied in a conventional way, as in modern structures, is often not feasible for historical structures (Roca, 2006). Therefore, case-based solutions need to be developed for conservation, strengthening, and retrofitting of heritage structures. For this purpose, a set of qualitative (such as inspection and historical research) and quantitative (such as monitoring and structural analysis) activities should be carried out. Quantitative analysis requires a structural model, which is constituted from a set of hypotheses on the mechanical response of the structure, material properties, internal morphology, and structural configuration (Roca, 2006). The structural model needs to be calibrated by means of empirical evidence in order to validate the adopted hypotheses.

[1] ISISE, Department of Civil Engineering, University of Minho, Azurém, 4800-058 Guimarães, Portugal

[2] Department of Civil Engineering, Eskişehir Technical University, 26555 Eskişehir, Turkey

[*] Corresponding author

e-mail: id8027@alunos.uminho.pt

Even so, constructing a realistic structural scheme with a precise description of the historical structure is hardly possible, independent of the effort made during the visual inspection and experimental descriptions (Roca, 2006). Heritage buildings are complex structures, and the seismic performance of these buildings is influenced by heterogeneous material distribution, sophisticated geometric features, limited information on the connections between structural components, building condition under long-term effects, and flexible horizontal elements which do not provide a global structural behavior, also often addressed as box-behavior (Lourenço et al., 2011).

In the present paper, Kütahya Kurşunlu Mosque in Turkey was investigated in detail. Construction of Kütahya Kurşunlu Mosque dates back to 1377-1378, using ruins of a pre-existing building, and the Mosque suffered several conservation and restoration interventions between the 13th and 19th centuries. In 2013, the Directorate General of Foundations of Turkey started restoration works and seismic retrofitting actions on the Mosque to address architectural and structural concerns. The main objective of the present study is to investigate the seismic performance of the Mosque—located in Kütahya province with a high seismic exposition—before and after it has been retrofitted. As per AFAD (2018), the peak ground acceleration (PGA) value of the recorded earthquake ground motions ranges between 0.22g and 0.53g for Kütahya province. Three earthquakes with high intensities occurred in Kütahya in March and April 1970 and in May 2011 (Table 1). Accordingly, the structure has experienced high seismic activity in the last 50 years, which, combined with past long-term effects on the structure, enforces both the study over the current condition of the Mosque and over the effectiveness of the retrofitting technique adopted—aiming to ensure safety for future events.

Table 1. Past events with high intensity in Kütahya (KOERI; Yılmaz and Avşar, 2013).

Date	Location	Mercalli Intensity	Magnitude Ms	Death Toll	Number of Damaged Buildings	Distance between the epicenter & the Mosque (km)
28.03.1970	Gediz-Kütahya	IX	7.2	1086	19291	≈ 70
19.04.1970	Gediz-Kütahya	VIII	5.8	-	1360	≈ 70
19.05.2011	Simav-Kütahya	VI	5.9	3	1500	≈ 90

2 Historical Kütahya Kurşunlu Mosque

2.1 Structural Description

Kütahya Kurşunlu Mosque is located in the residential area of the city, but it is not attached to any building. The Mosque has a rectangular plan with a length of 13.0 m and width of 9.3 m (Fig. 1, and Fig. 2). The highest element of the Mosque is the minaret, with a height of 28.0 m, and it has a rectangular base with a polygonal transition section to a circular body. In the main body, the height of the load-bearing walls, which were constructed as three-leaf masonry, and the top point of the dome are 7.8 m and 11.0 m, respectively. The construction material of the Mosque is cut stone and brick, and the outer layer of the walls was built with cut stone; whereas rubble stone was used for the inner layer and core of the load-bearing walls. The dome, which is restrained by an octagonal drum, the vaults, pendentives, and octagonal drum were constructed using brick. The minaret base and circular body are constituted with cut stone and brick, respectively.

(a) (b)

Fig. 1. Kütahya Kurşunlu Mosque after interventions: (a) south façade, (b) east and north façades

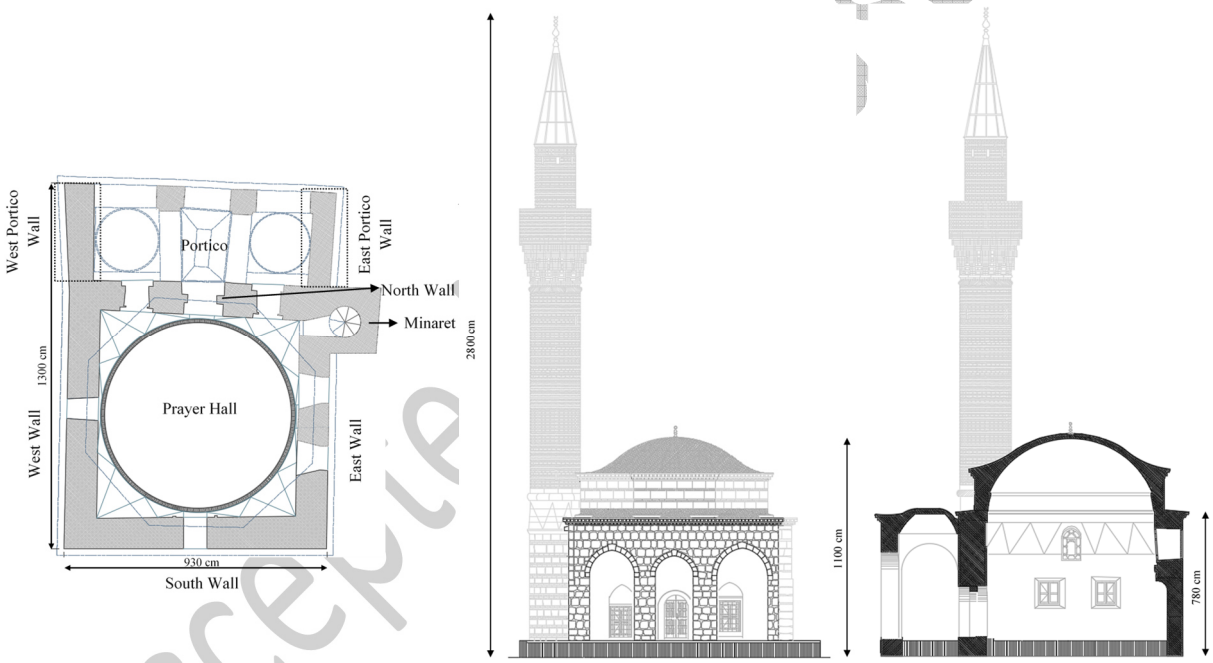

(a) (b) (c)

Fig. 2. Geometry of the Mosque: (a) plan, (b) north elevation, (c) section cut of the east elevation

2.2 Damage Survey

In-situ inspection plays an important role on the seismic assessment of historical constructions aiming to identify the condition of the building and define a representative structural model. At the time of the inspections, restoration of the minaret had already been completed, and no damage was reported. In the Mosque, wooden tie beams were used on the arch elements of the portico to overcome the developed thrust at the arch springing. Some of these tie beams were missing, and others were subjected to deterioration (Fig. 3(a)). Moreover, large cracks were observed on the load-bearing masonry walls. A significant crack which propagates vertically from the top level of the wall façade was reported on the south wall (Fig. 3 (b)). Additionally, loss of wooden tie beams was reported, and vertical cracks were observed on the masonry walls around the window openings (Fig. 3(c)). On the west façade

of the Mosque, a moderate vertical crack was noted, the location of which corresponds to the intersection of the two perpendicular walls—the north wall and the west prayer hall wall—and west portico wall (outer leave, Fig. 3(d)). The damage can be related to the lack of connection between structural elements. Another moderate crack was observed in the middle of the west portico wall (inner layer, see Fig. 3(d)).

Furthermore, vertical cracks were observed on the octagonal drum, both at the interior and exterior surfaces (Fig. 3), and expansion of the octagonal drum is expected due to out-of-plane movement of the structural walls which support it. In fact, lack of global structural behavior of the Mosque contributed to the cracks observed on the octagonal drum followed by the crack propagation on the dome. As given in Fig. 4, extensive damage is reported not only on the intrados but also on the extrados when the lead surface cover of the dome was removed. The stability of the dome is, given the existing crack pattern, uncertain for the future seismic events.

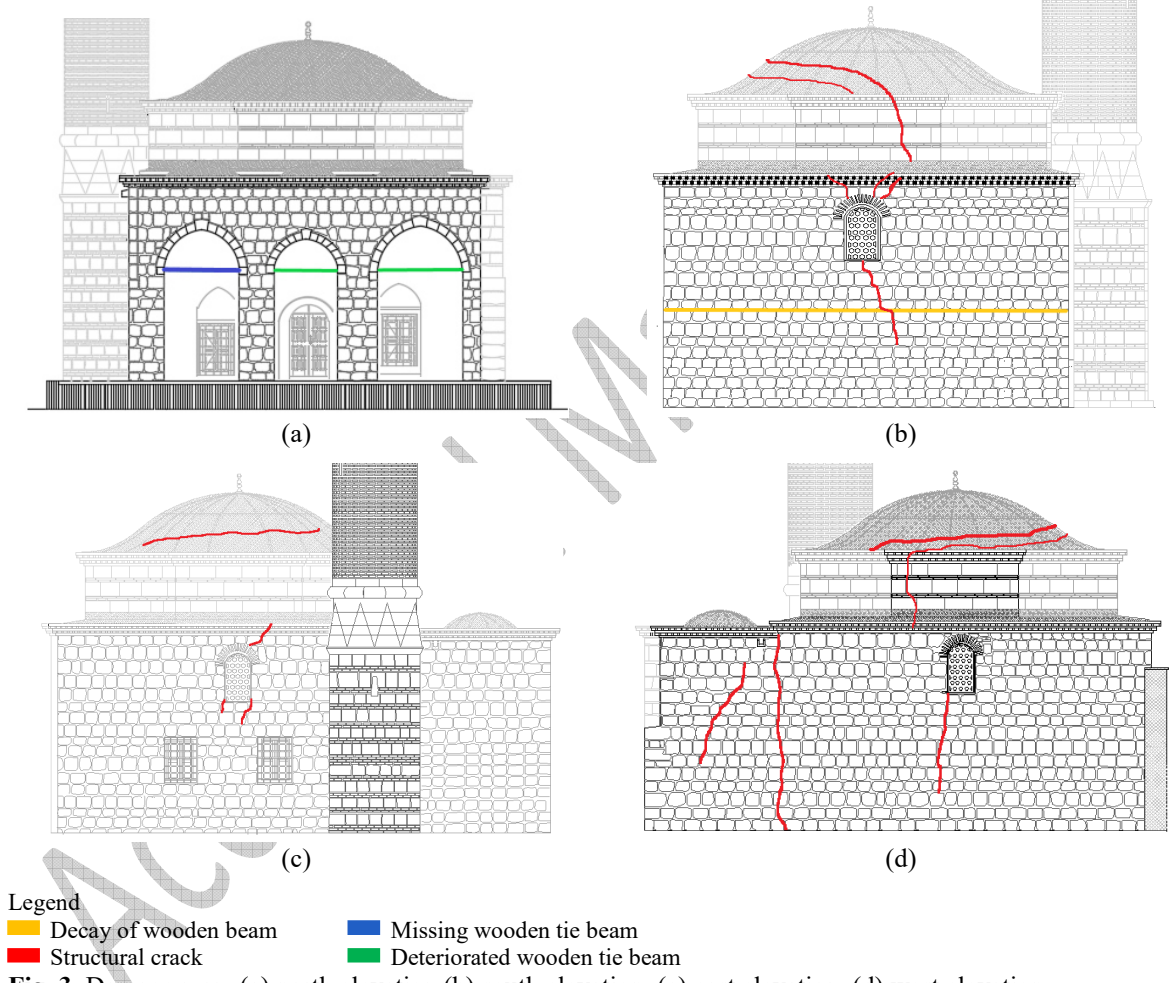

Fig. 3. Damage map, (a) north elevation (b) south elevation, (c) east elevation, (d) west elevation

Fig. 4. Large cracks observed on the dome exterior and interior

2.3 Steel Girder Retrofitting

Seismic retrofitting is crucial to such a structure with severe cracks and located in a high seismic prone zone. A steel girder retrofitting was decided by the Directorate General of Foundations based on the damage observed on the dome and the structural walls. The principle of minimum interventions and reversibility was taken into account, even if different solutions were possible. The configuration of the steel girder retrofitting is given in Fig. 5. Steel elements having U160 section were inserted at the top level of the walls to improve the interaction between the structural walls. In the past, wooden beam elements were used on masonry structures to provide tensile capacity. Once the old brick material was removed from the bottom of the drum, total loss of wooden beam elements was reported, as seen in Fig. 6(a), and the loss of the ties contributed to the cracks observed on the dome. Thus, single U160 steel girder elements were placed not only at the base section of the drum (Fig. 6) but also at the top of the drum walls (Fig. 7). Its introduction encompasses several considerations, such as: (a) steel elements were welded to ensure rigid connections; (b) afterwards, the gap between the steel elements and the masonry was filled with hydraulic lime-based mortar; (c) the steel elements were covered by masonry units compatible with the old material; and (d) the steel elements at the top of the drum wall were connected to the masonry by steel anchors (Fig. 7(b)). It is expected that these steel elements provide additional tying to the dome and limit the expansion of the existing cracks in case of any future action.

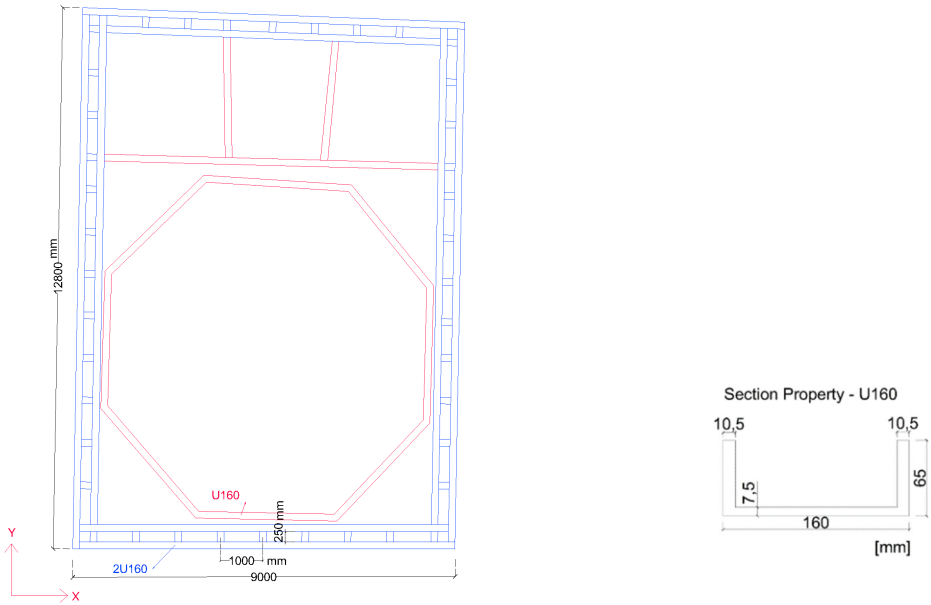

Fig. 5. Steel girder application plan

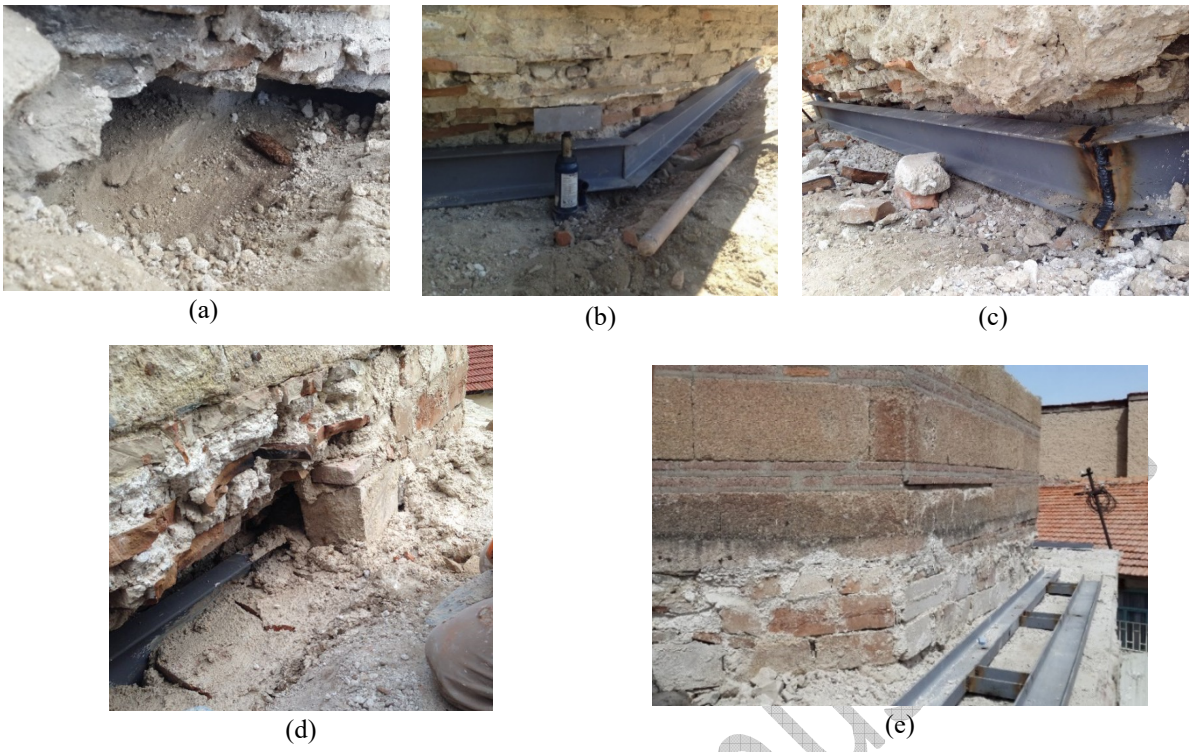

(a) (b) (c)

(d) (e)

Fig. 6. Implementation of the steel girders at the bottom level of the drum, (a) loss of wooden beams, (b) steel girder elements placed at the bottom section of the drum, (c) welded connection of steel girder elements, (d) hydraulic lime-based injection and covering, (e) covering the elements with new masonry material

(a) (b)

Fig. 7. Steel girder elements at the top of the drum, (a) single U160 elements, (b) steel anchor connection

The steel girders were anchored at the top level of the load-bearing walls aiming to provide interaction of the structural walls (Fig. 8). Single U160 was anchored on the north wall, whereas double U160 steel elements were implemented to the rest of the load-bearing walls (see Fig. 5). All steel elements were fixed to the walls using steel anchors after hydraulic lime-based injection was applied to the anchor holes. Additionally, parallel double steel profiles were connected using U160 every meter (Fig. 8). Finally, steel girders were covered with mortar, and the dome top surface and portico was coated with lead, as shown in Fig. 9.

Fig. 8. Application of double steel girder (2U160) on the load-bearing walls

Fig. 9. Lead covering after steel girder retrofitting

3 Numerical Modelling

3.1 Generation of the Finite Element Model

A representative structural scheme of the Mosque was constructed through a 3D finite element numerical model using the software Midas FX+ for DIANA. A simplified geometry of the Mosque was considered in the modelling, adopting the so-called macro-modelling approach, which assumes homogenous material behavior (Lourenço, 2002). The numerical model includes the majority of the structural volume, as seen in Fig. 10. The masonry minaret was excluded since no structural damage was reported. As stated in Silva et al. (2018), a three-dimensional numerical model composed of solid elements with fine meshing is preferable to represent such heritage structure with complex geometry. This strategy was adopted in several studies, namely Karanikoloudis and Lourenço (2018), Kazaz and Kocaman (2018), Kocaman et al. (2018), Ciocci et al. (2018), Valente and Milani (2018), and Almac et al. (2016). However, this strategy requires much computational effort for nonlinear analysis in the dynamic range. An optimized numerical model of the Mosque was prepared by using, as needed, beam, shell, and solid elements in the present work (Fig. 10). A set of beam elements (L13BE) was used to represent steel girder elements on the retrofitted model. Shell elements (triangular T15SH) constituted the load-bearing walls, arcades, piers, dome, drum, and pendentives above the portico. A set of solid elements (tetrahedron TE12L) were used to model the geometry of the pendentives, as they have a complex volume geometry (Fig. 10(e)). Lintel elements were also considered, as addressed in Lourenço et al. (2007).

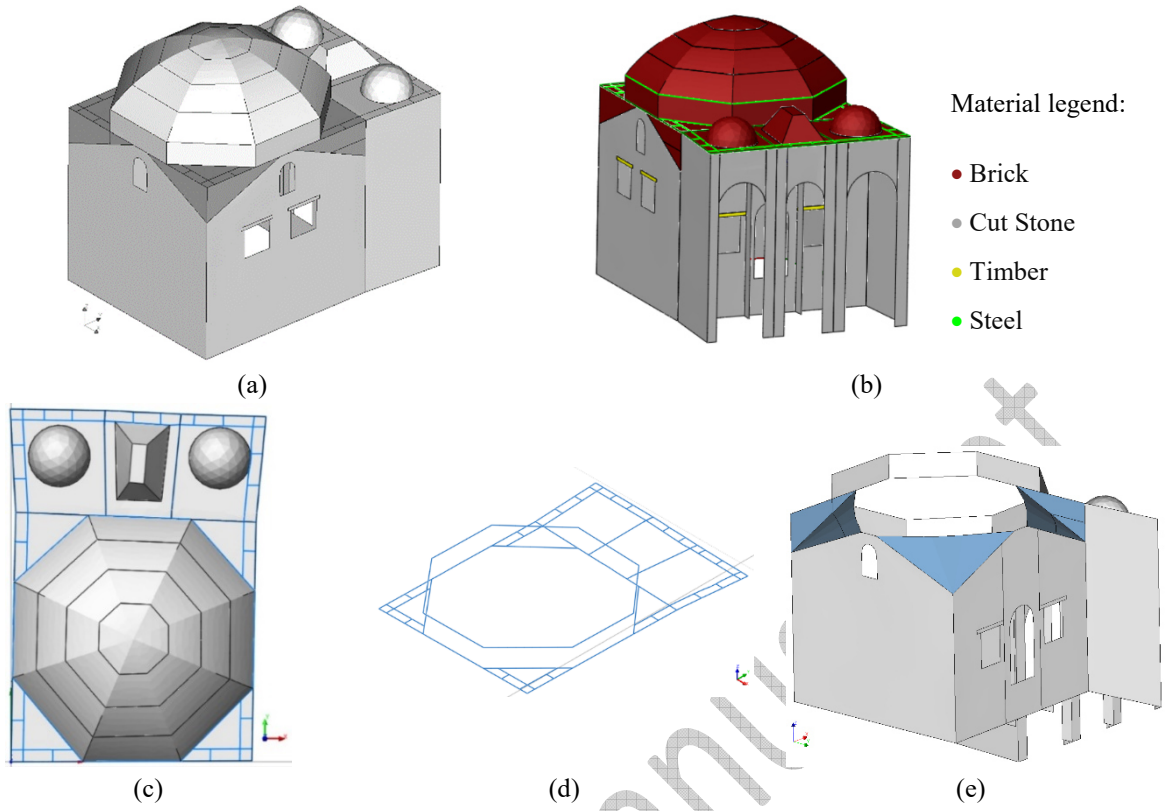

Fig. 10. Numerical model of the Mosque, (a) three-dimensional model, (b) identification of the materials, (c) top view, (d) configuration of the steel girder retrofit, (e) simplified geometry of the pendentives as solid elements (colored as blue)

The definition of the Mosque geometry was achieved through the provided architectural drawings and site measurements performed. The south, east, and west main walls and portico walls have 1000 mm thickness, while north wall has a thickness given by 1200 mm. In the numerical model, the maximum thickness of the drum considered was 800 mm, and four different sections having thickness varying between 500 mm and 200 mm, tapered to the top, were defined to have better representation of the dome geometry. There is no experimental evidence available for the mass of the dome. Despite the fact that mass is usually concentrated in vertical elements (walls) in historic structures, a sensitivity analysis was performed to investigate the effect of the dome mass on the global modal response. A 20% reduction in density results in a maximum difference of 1.5% for the frequency, and such deviation seems negligible. The adopted triangular mesh size was considered as 300 mm for the dome, drum, pendentives, and vaults, while a finer mesh size of 200 mm was defined for the load-bearing walls and arcades in order to minimize convergence problems affected by mesh size and mesh distortions during nonlinear analysis. The numerical model of the retrofitted Mosque has 27,250 elements, in which 428 are beam elements, 22,978 are triangular shell elements, and 3,844 are tetrahedral solid elements, with a total of 12,892 nodes and 72,950 degrees of freedom. The degrees of freedom located at the foundation of the structural system were assumed as fully fixed.

3.2 Material Properties

Physical nonlinear behavior was defined by the total strain fixed crack model, provided in TNO DIANA (2017). The constitutive model is defined by means of the stress-strain relationship for tension and compression, see Fig. 11. The tensile behavior of the masonry is assumed to have exponential stress-strain relation beyond the tensile

strength, whereas the compressive behavior is adopted to be parabolic for both hardening and softening relation. Both tension and compression softening curves are based on fracture energy and its relationship with the crack bandwidth (h) of the element. After the onset of cracking, the shear stiffness has been reduced by a shear retention factor with a value given by 0.01 to limit the shear stress increase. The material properties adopted in the numerical model are gathered in

Table 2. The Young's modulus values were calibrated considering the data retrieved from the performed modal identification analysis, as detailed later in the paper. Since direct characterization tests of the construction materials were unavailable, the nonlinear material properties related with strength were estimated according to the Italian Code (2009). For the compressive strength values, the Italian Code (2009) recommends a range of 2.6 MPa – 3.8 MPa and 6.0 MPa – 8.0 MPa for cut stone masonry and masonry of squared stone blocks, respectively. Taking into account the calibrated Young's modulus values, the minimum values of the latter intervals were defined. It is also noted that historical buildings (given the low level of compressive stresses and very low tensile strength) are often controlled by the geometry, making compressive strength values less relevant. Tomaževič (1999) recommends a range of tensile strength values for existing stone and brick masonries, being herein assumed a value of 0.1 MPa for both masonry types (cut stone and brick). For the tensile fracture energy of masonry, a value of 0.012 N/mm is recommended (Angelillo, Lourenço, and Milani, 2014). For the compressive fracture energy (G_c), an average ductility index in compression (ratio between fracture energy and strength) is defined, and different limit values are obtained from Model Code 90 (CEB-FIP 1993) for different range of compressive strengths. A value of 1.6 mm is recommended for the ductility index in compression in which f_c values are lower than 12 N/mm^2 (Angelillo, Lourenço, and Milani, 2014). Therefore, the relation given in Eq. 1 was assumed to estimate the compressive fracture energy in the present paper. For the steel, material properties presented in Fig. 12 were assumed.

$$G_c = 1.6 \times f_c \qquad for\ f_c < 12\ MPa \qquad \text{Eq. 1}$$

It may be stressed that, given the multiple uncertainties of the model, the obtained numerical global capacity of the historic structure requires careful analysis. Nevertheless, the results obtained here allow, certainly, an important comparison between the retrofitted and non-retrofitted models.

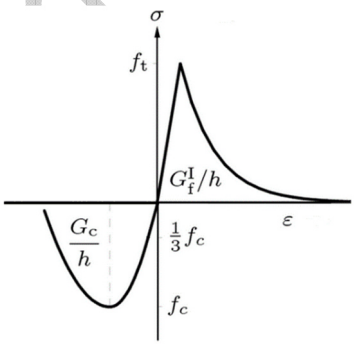

Fig. 11. Stress and strain relations of the tensile and compressive behavior of the material adopted in the total strain crack fixed model (TNO DIANA 2017)

Table 2. Mechanical properties of the materials

Material	γ (t/m³)	E (MPa)	υ (Poisson ratio)	Compressive strength (f_c) [MPa]	Tensile strength (f_t) [MPa]	Compressive fracture energy (G_c) [N/mm]	Tensile fracture energy (G_t) [N/mm]
Cut Stone	2.1	1500*	0.2	2.6	0.1	4.2	0.012
Brick	2.0	2500*	0.2	6.0	0.1	9.6	0.012
Timber	0.7	11000	0.3	-	-	-	-
Steel	7.85	200000	0.3	235	235	-	-

*Obtained from dynamic identification

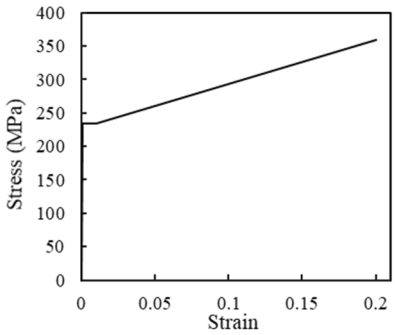

Fig. 12. Stress-strain relation adopted for the steel material in the FE model

4 Identification of Modal Parameters

Dynamic-based modal identification includes theoretical and experimental modal analyses. Firstly, an ambient vibration test was performed on the Mosque using environmental vibrations as a source of excitation. One accelerometer was placed in a fixed point—namely a reference station—while another accelerometer was relocated to seven different points on the top of the load-bearing walls. Approximately 20 minutes were spent at each station, whereas the reference station was continuously operated during the measurement. The location of each station on the Mosque is given in Fig. 13, and locations of the stations were decided from the modal response of a preliminary numerical model to identify in-plane and out-of-plane movement of the components. In order to perform ambient vibration tests, two digital triaxial accelerometers were used. The accelerometers have a frequency range of DC-100 Hz with a sensitivity range from ±0.1 to ±4.0g and 10 V/g of resolution. Additionally, a data acquisition system with 24 bits resolution was used for collecting the data.

Following that, Operational Modal Analysis (OMA) was performed, and experimental modal parameters were extracted using ARTeMIS Modal software. Two different signal processing methodologies were carried out, namely Enhanced Frequency Domain Decomposition (EFDD) and the Stochastic Subspace Identification – Unweighted Principal Components (SSI-UPC), and the latter was considered and presented as the experimental modal response of the Mosque. Both methods can be applied, and there is no strict application of one methodology because the reliability of the results depend on the environmental noise, structural components, quality of measurement of the system, and technical expertise from the experimental campaign personnel (Aguilar et al., 2012). However, Ramos, Aguilar, and Lourenço (2010) noted that results of the non-parametric methods, which EFDD is defined as, depend on the quality of the environmental noise, and such drawback can be overcome by using parametric methods, i.e. SSI-data. Numerous studies have been performed using experimental modal identification tests on historical structures. For instance, Gentile and Saisi (2007) performed ambient vibration measurements and identified five vibration modes of a masonry tower. Aguilar *et al.* (2012) performed OMA on a Peruvian Historical Building and identified the first two translational modes and seven subsequent local modes

of the building. Nohutcu *et al.* (2015) conducted free vibration tests and calibrated representative numerical model of a historical Mosque with 1% error for the average differences of the first five vibration frequencies. Sevim *et al.* (2011) applied an experimental modal testing to a historical masonry arch bridge, and the frequencies of four modes have been correlated with up to 2% error. Lourenço *et al.* (2012) performed a study of seismic performance and safety-level identification of masonry ruins, where a modal testing was carried out by using environmental noise as excitation source in order to update finite element model and have a representative structural scheme. Accordingly, a methodology based on operational modal analysis is feasible and even effective to identify damage on masonry-like structures (Ramos *et al.*, 2010).

In the present case study, the ambient vibration measurements were performed in 2017 after the intervention works, and, therefore, the numerical calibration step was performed over the retrofitted model. Specifically, an eigenvalue analysis was performed for a preliminary finite element model of the structure. The calibration was achieved by fitting the obtained numerical eigenvalues with the experimental ones through a trial and error approach. It may be stressed that the OMA allows the calibration of the elastic structural behavior of the Mosque, meaning that only the elastic stiffness of the structure is suitable to be calibrated. Therefore, the Young's modulus of the masonry materials, i.e. cut stone and brick masonry, are considered to be the variable parameters within the calibration process. The latter comparison, in terms of numerical and experimental frequencies, and its relative differences are given in Table 3. The Modal Assurance Criterion (MAC) values were also determined to easily assess the quality of the obtained fitting (using as reference the modal shapes). Higher MAC values, generally greater than 0.8 and not lower than 0.4, are desired for each mode shape (Gentile and Saisi, 2007); however, the calibration process was carried out by prioritizing the minimization of the difference in frequency content. The average error of the first four frequencies is 4.9% for the calibrated model, which is considered to be satisfactory. However, the MAC values obtained for the second and third modes showed poor correlation. The final calibrated Young's modulus values were found to be 1500 MPa for cut stone and 2500 MPa for brick. Furthermore, the experimental and numerical mode shapes are presented in Fig. 14.

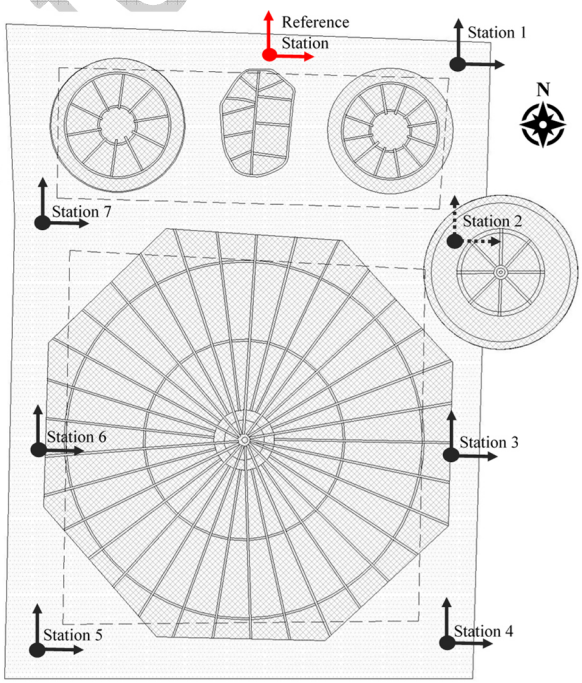

Fig. 13. Station layout and sensor directions

The first four numerical global frequencies range from 5.77 Hz to 11.32 Hz, with a cumulative mass participation ratio of 70.83% in the x-direction (transversal) and 67.28% in the y-direction (longitudinal). Considering 100 modes, it is possible to obtain a cumulative mass participation ratio of 90.35% in the x-direction, 89.84% in the y-direction and 82.69% in the z-direction, as given in

Table **4**. The first mode is global and translational in the x-direction, with torsional effect also observed due to the relatively high modal displacements between south and north façades. The second mode is also a translational mode, in the longitudinal (y-) direction of the Mosque, whereas the third mode is dominated by torsional movement. The fourth mode mainly involves out-of-plane movement of the structural walls and the drum, and, consequently, the dome is subjected to expansion or contraction.

Table 3. Comparison of the experimental and calibrated numerical modal frequencies

Mode	f_{exp} (Hz)	f_{num} (Hz)	Error (%)	Average Error (%)	MAC
1	5.72	5.77	0.9	4.9	0.75
2	7.85	7.87	0.2		0.40
3	10.69	9.77	8.6		0.51
4	12.55	11.32	9.8		0.85

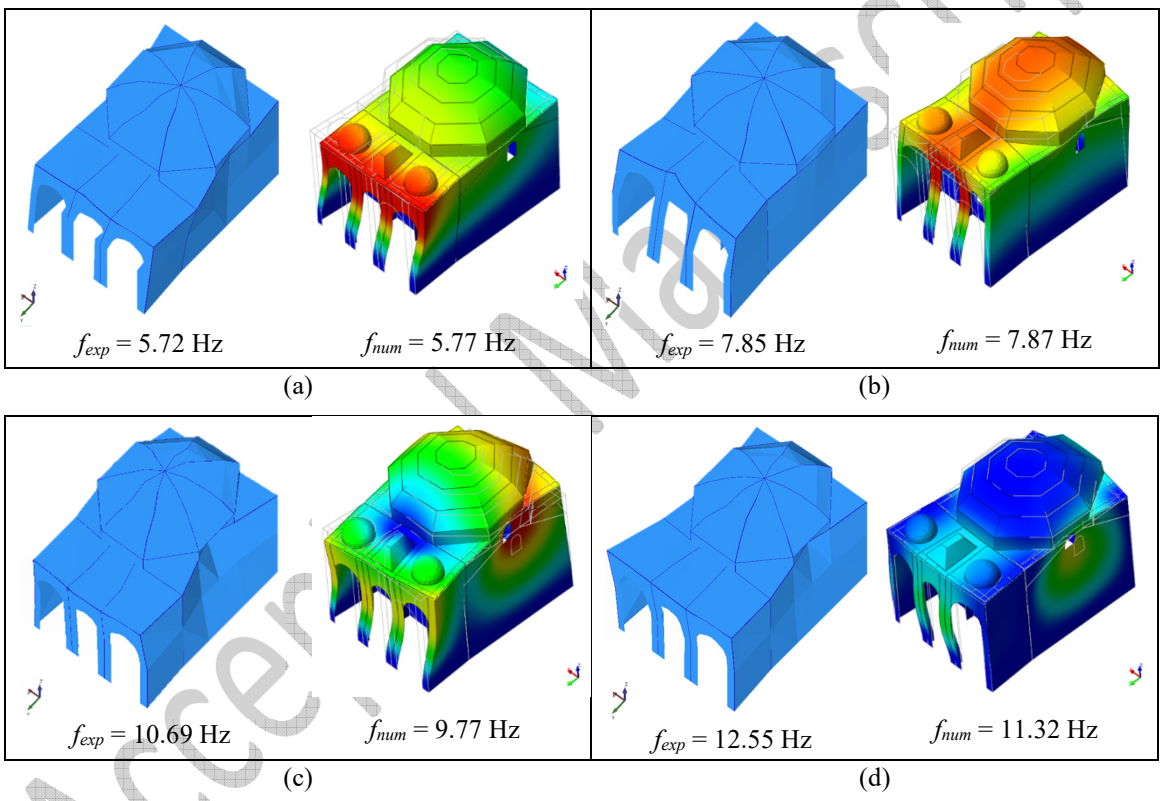

Fig. 14. Experimental and calibrated numerical modes of vibrations for the first four modes, (a) 1st mode, (b) 2nd mode, (c) 3rd mode, (d) 4th mode.

Table 4. Frequencies, periods and cumulative mass participation ratios of the retrofitted model in each direction

Mode	f (Hz)	Period (s)	Cumulative Mass Participation (%)		
			X component	Y component	Z component
1	5.78	0.17	60.72	≈ 0.00	≈ 0.00
2	7.87	0.13	61.13	66.95	≈ 0.00
3	9.77	0.10	70.80	67.27	≈ 0.00
4	11.32	0.09	70.83	67.28	≈ 0.00
100	59.32	0.02	90.35	89.84	82.69

It is important to mention that the non-retrofitted model is, in terms of geometrical and material properties, the same as the retrofitted model, the only difference being the existence of the steel girders on the latter model. In fact, frequencies, mode shapes, and cumulative mass participation ratios of the non-retrofitted model are quite similar with the retrofitted finite element model, and there is no significant change in modal response, as expected. Therefore, the non-retrofitted model was used to represent the nonlinear response of the non-retrofitted condition of the Mosque before damage. Damage was not considered in the numerical model due to the limited information about the internal damage and the lack of representativeness.

5 Seismic Assessment of the Kütahya Kurşunlu Mosque

5.1 Nonlinear Pushover Analysis

Nonlinear pushover analyses are usually preferred to perform the seismic assessment of a structure because less computational effort is needed when compared to the dynamic analyses and failure can be more clearly defined. The seismic assessment of the Mosque was first carried out by conducting nonlinear pushover analyses. The iterative solution method of the analysis was selected as secant method, and the arc-length control method was used for obtaining the peak load factor. Each equilibrium step was calculated according to the internal energy with a tolerance value of 0.001. The seismic forces were represented as horizontal loading proportional to the mass of the structure. The adopted loading pattern was also considered in several studies—for instance, Braga (2014), Lara (2016), Mangia et al. (2016), Karanikoloudis and Lourenço (2018), Ciocci et al. (2018), Silva et al. (2018). Monotonically increased lateral loads were applied after the structure was loaded with the gravity forces. A unidirectional mass proportional seismic action was implemented, and the seismic performance was studied in both positive and negative transversal and longitudinal directions of the Mosque. Several control points, which are presented in Fig. 15, were defined in order to develop the pushover curves by relating base shear coefficient (or load factor) and displacement of the control point. The base shear coefficient is the ratio between the sum of the acting horizontal forces and the sum of the vertical forces (self-weight). Pushover analyses were conducted for both numerical models with and without retrofitting, and a comparison of the capacity curves are presented. Furthermore, the maximum principal tensile strain distributions, which are good damage indicators, according to Mendes (2012), were investigated to compare the non-retrofitted model's damage pattern with the observed damage.

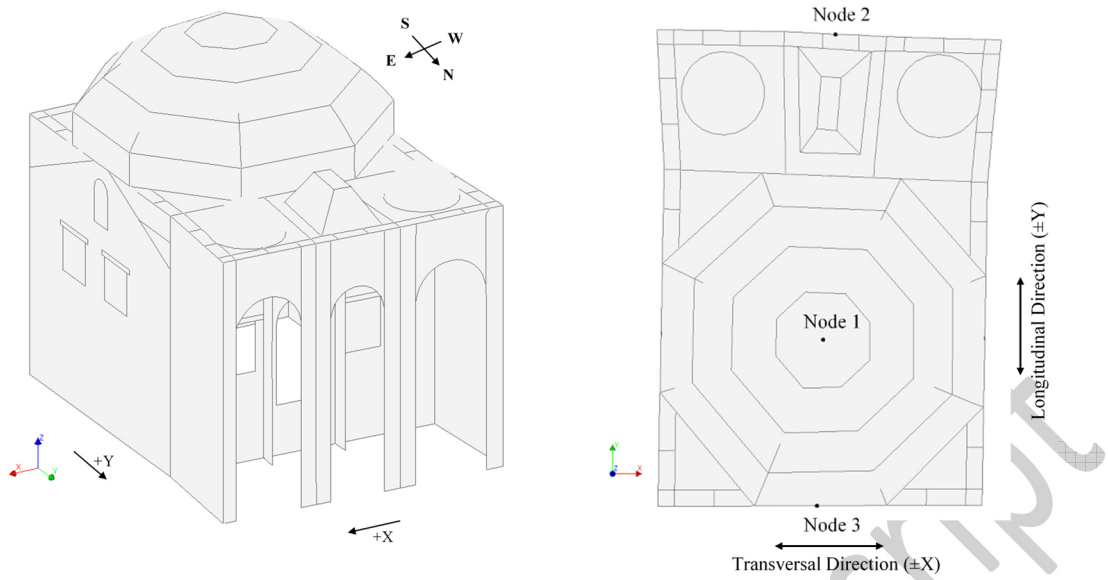

Fig. 15. Global coordinate system and defined control nodes, (a) global axes, (b) control nodes

The capacity curve of the Mosque was computed by considering three different control points—Nodes 1 and 2 for the transversal direction and Nodes 1 and 3 for the longitudinal direction. The control points were located on the top point of the dome, the highest level of the portico and the south wall, namely Nodes 1, 2, and 3, respectively (see Fig. 15). In Fig. 16(a), the pushover curves depict that the first crack initiates when a value of 0.18g horizontal load acted on the structure in the transversal direction. A similar cracking load was achieved for the non-retrofitted and retrofitted models, whereas the maximum lateral load in the x-direction was observed to be nearly 0.38g and 0.4g, respectively. The peak horizontal displacements are, for the non-retrofitted model, lower than the retrofitted one in the x-direction, and the post-peak ductility is much increased by the retrofitting.

A higher lateral load capacity was observed for the y-direction when compared to the x-direction. The results were expected since the area of the load-bearing walls is larger in this direction. Fig. 16(b) illustrates that the non-retrofitted representative scheme can resist a lateral load up to half of its total weight, and the capacity in the (-) y-direction increases to nearly 0.6g when the steel elements are introduced. Also, the retrofitting allowed increasing the lateral load capacity from a value of 0.48g to 0.56g for the (+) y-direction. Again, the ductility is increased enormously with the retrofitting.

Fig. 16 shows that the non-retrofitted model has a low capacity to dissipate energy—expected in historical masonry structures due to the quasi-brittle nature of the masonry. Likewise, the final loading step of the presented pushover curves do not represent the global failure of the historical Mosque, but the curves are sufficient to characterize and reproduce the local damage. On the contrary, the retrofitted model has a higher energy dissipation capacity. As the adopted seismic retrofitting improves the global response of the structure by achieving the so-called box-behavior, in-plane failure mechanisms dominate the global response and, therefore, allow a better redistribution of the imposed stresses and failure to be controlled by in-plane shear mechanisms. Similar conclusions have already been noted in different studies performed on historical structures—for instance, in Karanikoloudis and Lourenço (2018), Ciocci, Sharma, and Lourenço (2018), and Silva, Mendes, Lourenço, and Ingham (2018). It is stressed that the adopted modeling approach is unable to capture disintegration of the masonry walls during seismic loading, meaning that the designer must decide on the adequacy of the masonry arrangement to prevent disintegration or

take appropriate measures such as reinforced plasters to prevent this local phenomenon. The damage pattern for the retrofitted case is presented in Fig. 17, and progression of the damage presents smeared patterns, allowing excellent redistribution of cracking strains.

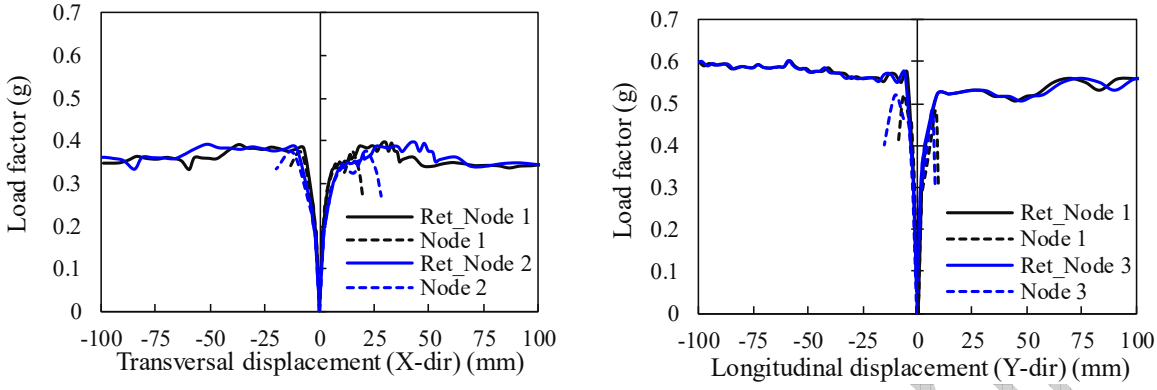

Fig. 16. The pushover curves of the non-retrofitted and retrofitted model in, (a) transversal direction, (b) longitudinal direction

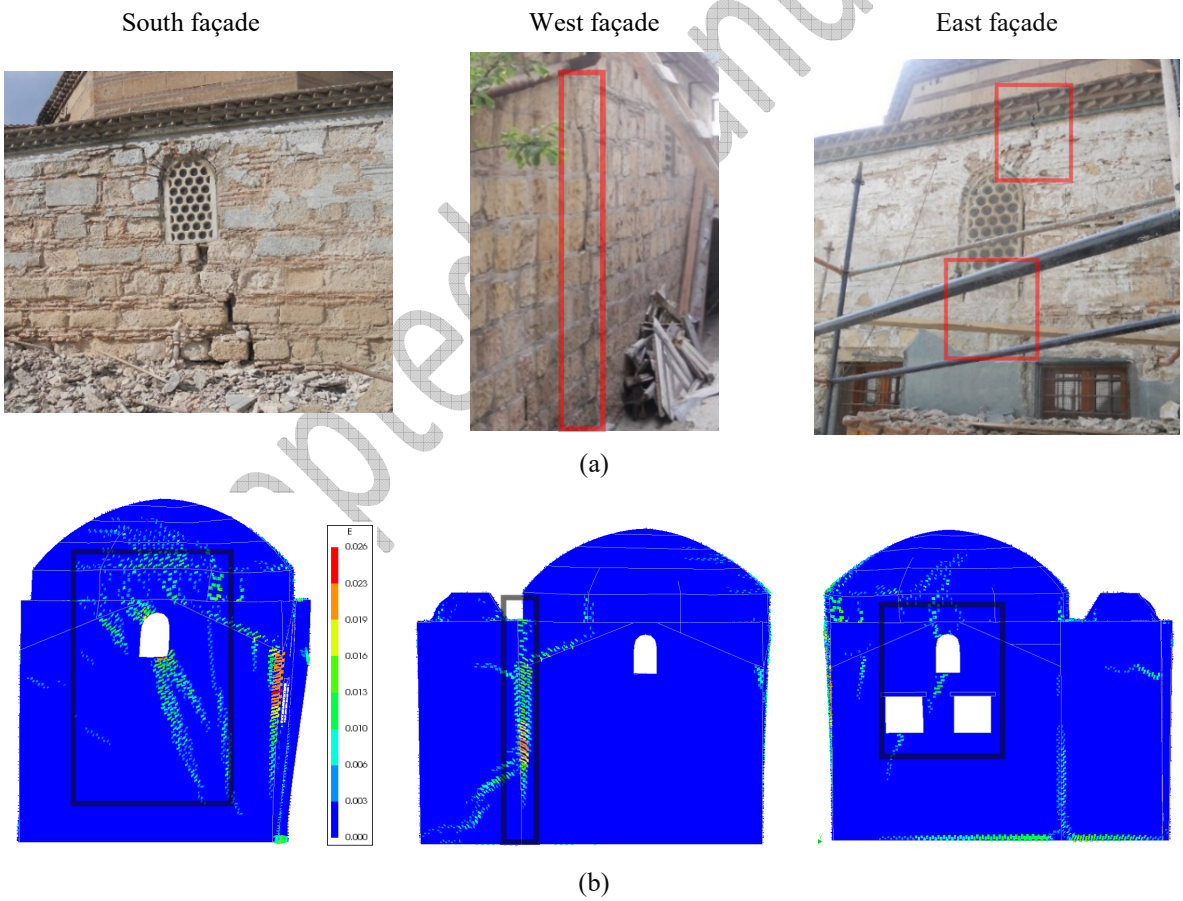

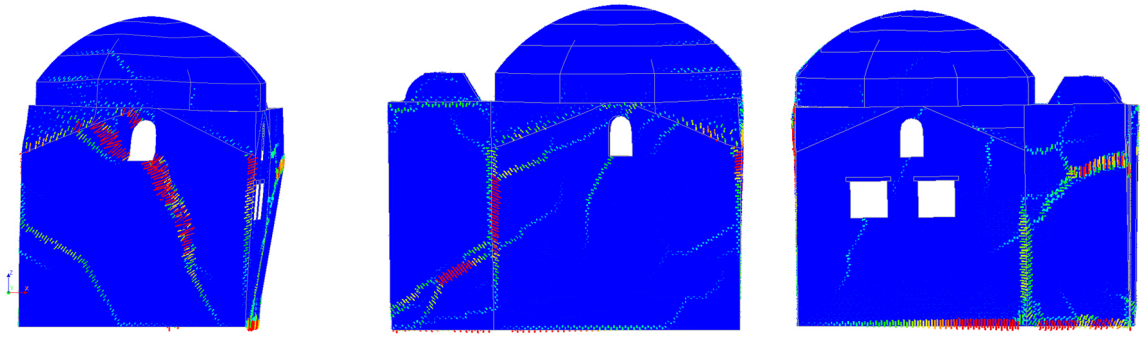

(c)

Fig. 17. Correlation between the numerical and real damage, (a) observed in-situ damage; (b) damage pattern for the retrofitted case in terms of maximum principal strain distribution for a lateral load 0.27g (post peak) in the (+)x-direction, (c) damage pattern for the retrofitted case in terms of maximum principal strain distribution for a lateral load factor of 0.39g (displacement 30.5 mm) in the (+)x-direction

The damage distributions shown in Fig. 17 depict similar patterns on the non-retrofitted model that are compatible with the observed damage in which the consistency of the numerical model can be validated. As given in Fig. 17(b), lateral loading in the (+) x-direction resulted in diagonal crack on the south wall in which in-plane behavior was observed. Additionally, a vertical crack seems to be originated due to the lack of interaction between the orthogonal structural components and the west and north walls. Similarly, Fig. 18 shows that vertical cracks appeared on the load-bearing walls that are connected orthogonally (at the intersection of the north, west, and west portico walls) as a result of the load subjected in (+) y-direction. In fact, it was observed that the first crack initiated at the pendentive and was further developed by the separation of the adjacent components in the numerical model (referring to the vertical crack) due to the lack of connection of the members. Furthermore, the vertical crack just below the window opening on the west wall can resemble the damage observed under the static loading in (+) y-direction. The damage obtained on the dome seems to be originated by the in-plane mechanism of the transversal walls and out-of-plane movement of the longitudinal walls in the (+) x- and (+) y-directions (Fig. 19). The strain plots present a similar cracking pattern to the observed damage on the outer and inner surfaces of the dome (see Fig. 4).

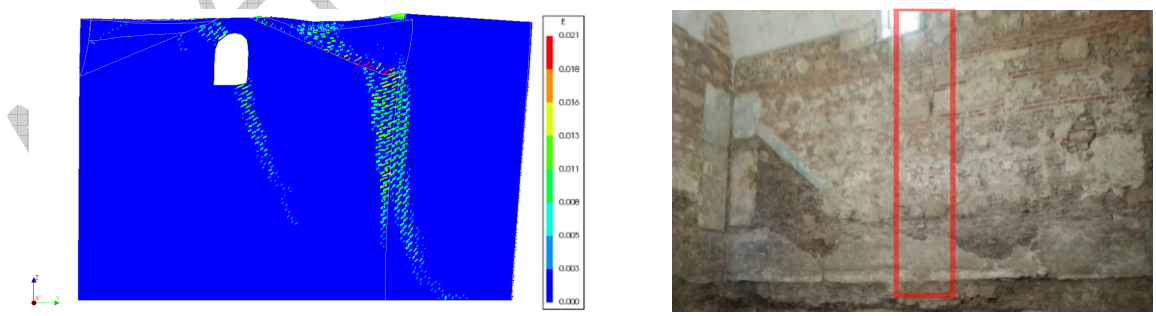

Fig. 18. Correlation of the numerical and real damage on the west wall of the non-retrofitted case in terms of maximum principal tensile strain distribution at load factor 0.3g in (+) y-direction

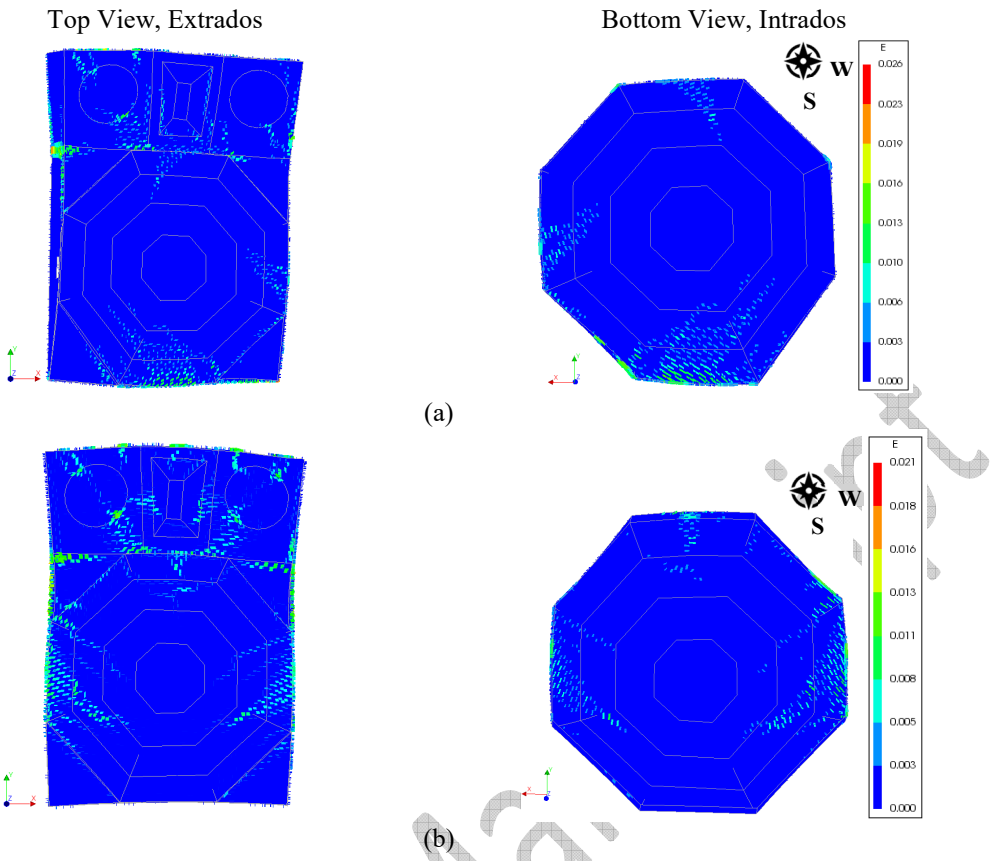

Fig. 19. Numerical damage on the dome of the non-retrofitted case in terms of maximum principal strain distribution (a) at load factor 0.27g in (+) x-direction, (b) at load factor 0.3g in (+) y-direction

5.2 Nonlinear Dynamic Analysis

The seismic assessment of the historical masonry Mosque is also studied by performing nonlinear response history analysis. The analyses were carried out for a set of three different earthquakes in which only horizontal seismic components were considered. Ground motions from past earthquakes occurred in Turkey were used to perform nonlinear dynamic analysis. According to TEC 2007, a minimum of three ground motions are required to perform an analysis in the time domain. Thus, three earthquakes were chosen from the Strong Ground Motion Database of Turkey (TR-NSMN), which is operated by the Earthquake Department of Disaster and Emergency Management Authority of Turkey. The seismological properties of each ground motion are given in Table 5. The given earthquakes, whose PGA values range from 0.28g to 0.82g, are among the most destructive earthquakes occurred in Turkey so far. In Fig. 20, the longitudinal and transversal components of each accelerogram are given, and Fig. 21 illustrates the response spectra of the input motions and the elastic response spectra defined in TEC 2007. The viscous damping ratio of Kurşunlu Mosque was assumed as 3%, as admitted in other studies (Kazaz and Kocaman, 2018; Ciocci et al., 2018) in which a Rayleigh damping strategy has been adopted during the nonlinear response history analyses.

Similar to other studies (Braga, 2014; Ozturk, 2017; Kazaz and Kocaman, 2018; Ciocci et al., 2018), the orthogonal components of each input motions were applied orthogonally to the global coordinate axes of the Mosque. The orthogonal component of each input ground motion with higher spectral acceleration value at the first vibration mode of the Mosque was applied through the transversal direction, which is the weak axis of the Mosque according to pushover analyses results (Fig. 21). Thus, transverse components of Erzincan and Bolu records and longitudinal

component of the Bingöl record were performed in the transversal direction (+x) of the Mosque, while other components of the input were acted in the longitudinal direction (+y).

Table 5. Seismological properties of selected ground motions (TR-NSMN)

Earthquake	March 13,1992 Erzincan	November 12, 1999 Düzce	May 1, 2003 Bingöl
Station Location	Meteorology Building *Erzincan*	MPWR Building *Bolu*	MPWR Building *Bingöl*
Station ID	2402	1401	1201
Epicentre Coordinates	39.72°N, 39.63°E	40.79°N, 31.217°E	38.94°N, 40.51°E
Station Coordinates	39.752°N, 39.487°E	40.746°N, 31.607°E	38.897°N,40.503°E
Depth (km)	23	11	6
Mw	6.6	7.1	6.3
Site Conditions – Soil Type (Kalkan and Gülkan, 2004)	Soil	Soil	Stiff Soil
Longitudinal PGA (g)	0.413	0.754	0.556
Transverse PGA (g)	0.480	0.821	0.282
Longitudinal PGV (cm/s)	108.0	56.6	34.5
Transverse PGV (cm/s)	78.2	66.9	21.9
Longitudinal PGD (cm)	34.4	25.2	10.2
Transverse PGD (cm)	29.5	12.8	5.1

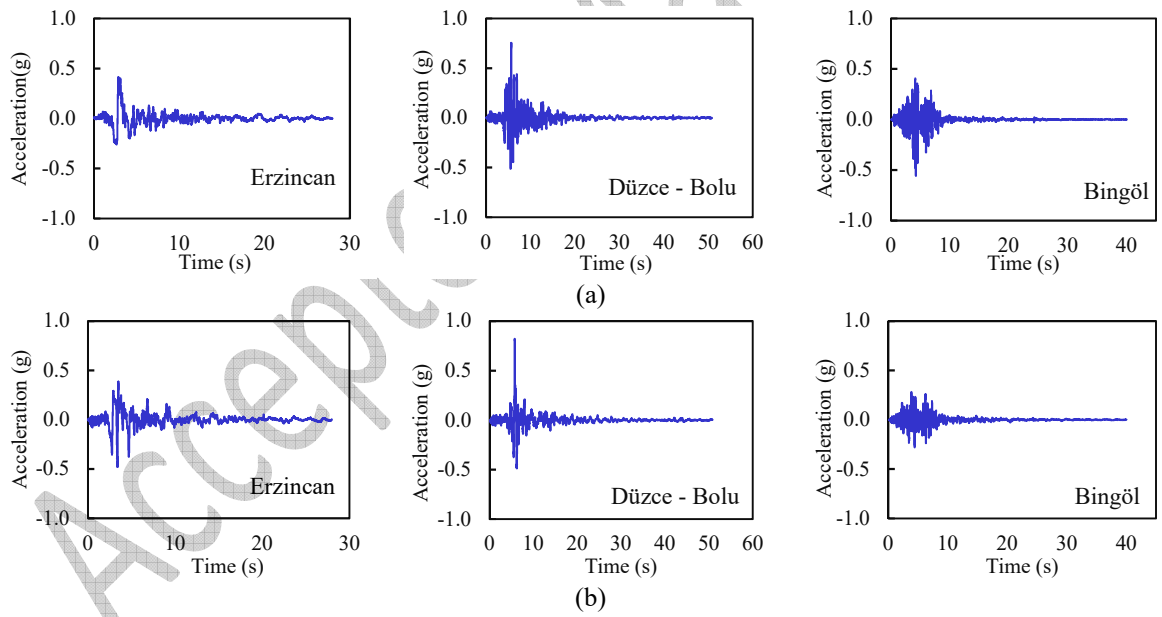

Fig. 20. Acceleration-time series of each record (TR-NSMN), (a) longitudinal component (N-S), (b) transversal component (E-W)

Since nonlinear response history analyses require high computational efforts, only a part of strong ground motion was considered in this study, aiming to speed-up the analyses. Thus, the duration of each record was shortened according to the cumulative energy duration that is proposed by Trifunac and Brady (1975), meaning that the time period under interest is in between the 5% and 95% of the total arias intensity energy. In this case, for the time instant of 20 s, the energy content of the motion reaches almost 100% of the total, and, therefore, only the first 20 s of each acceleration-time series was considered in the dynamic analyses.

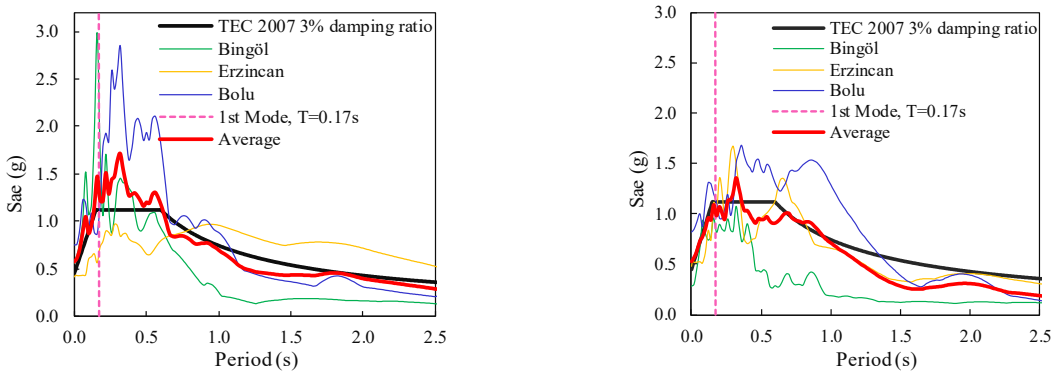

Fig. 21. Elastic response spectra of input records and design spectrum, as per (TEC 2007) for Z3 soil condition, (a) longitudinal components (N-S), (b) transverse component (E-W)

5.2.1 Change in the out-of-plane displacement

The change in the out-of-plane displacement with respect to time at each control node is given in Fig. 22 and Fig. 23 for both transversal (x) and longitudinal (y) directions, respectively. These figures consider parallel walls on the same plot to identify the movement direction of the components whether they are involved in a global structural behavior. The response at the two control points on the east and west walls have similar trends, but both control nodes present residual displacements in the opposite direction, as shown in Fig. 22. It is obvious that the steel girder retrofitting mitigates residual displacements. The displacements history of the nodes has a similar trend and amplitude, which can be an indication of the global structural behavior improvement. In general, a considerable decrease in the peak displacement was observed in the Erzincan and Bingöl cases. Although a reduction in the peak displacement was observed in Fig. 22(b) and Fig. 23(b), the imposed displacement values are still high and can be an indication of structural damage.

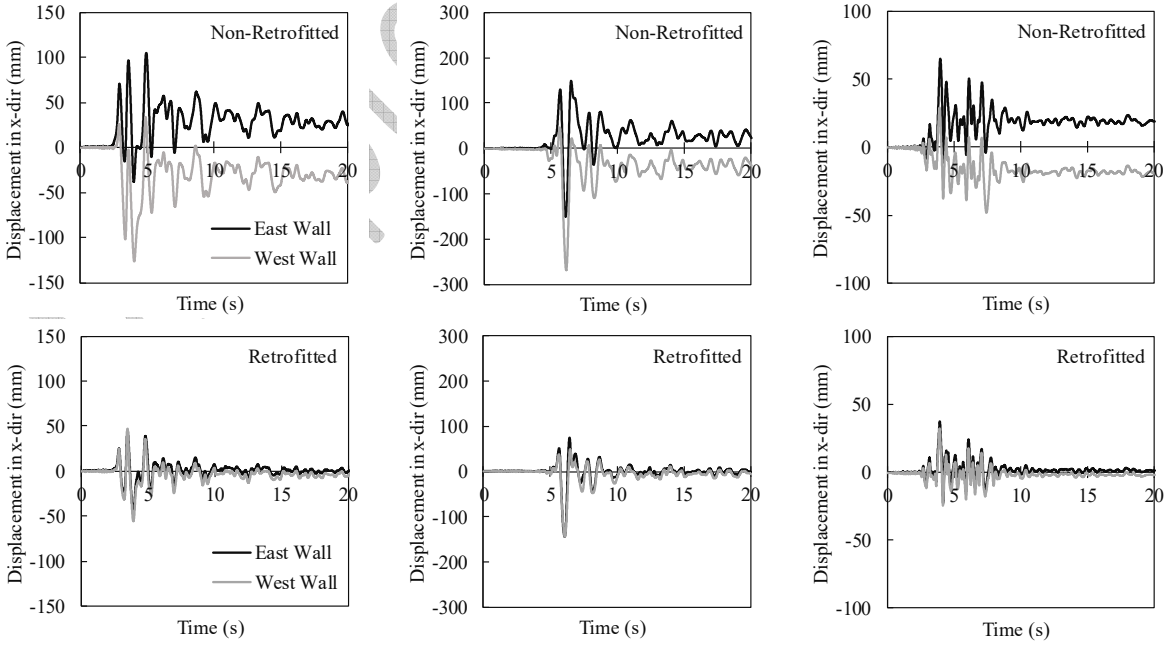

Fig. 22. Displacement-time series of control nodes at east wall and west walls for three ground motions in x-direction, (a) Erzincan, (b) Düzce – Bolu, (c) Bingöl

Displacement-time series and peak displacement at each control point at the top level of the walls may not be representative of the change in response. Therefore, the displacement response in the out-of-plane direction along the height of the structural walls (west/east), for transverse action, were plotted as an example. In order to plot these curves, a time-step of the peak displacement response which occurred at the control point on the non-retrofitted model was considered, and the vertical section of the mid-length of the wall was considered as the section cut (Fig. 24(d)). In all plots, the section above 7.8 m represents the drum where the dome is supported. However, there is no significant change in relative displacement on the drum section. Due to the fact that two parallel walls do not have maximum out-of-plane displacements at the same time-step, only the time-step when the west wall has the maximum displacement were presented in this paper, as given in Fig. 24. Again, it is clearly seen that implementing steel girders allow reducing the observed out-of-plane displacement of the walls along the height.

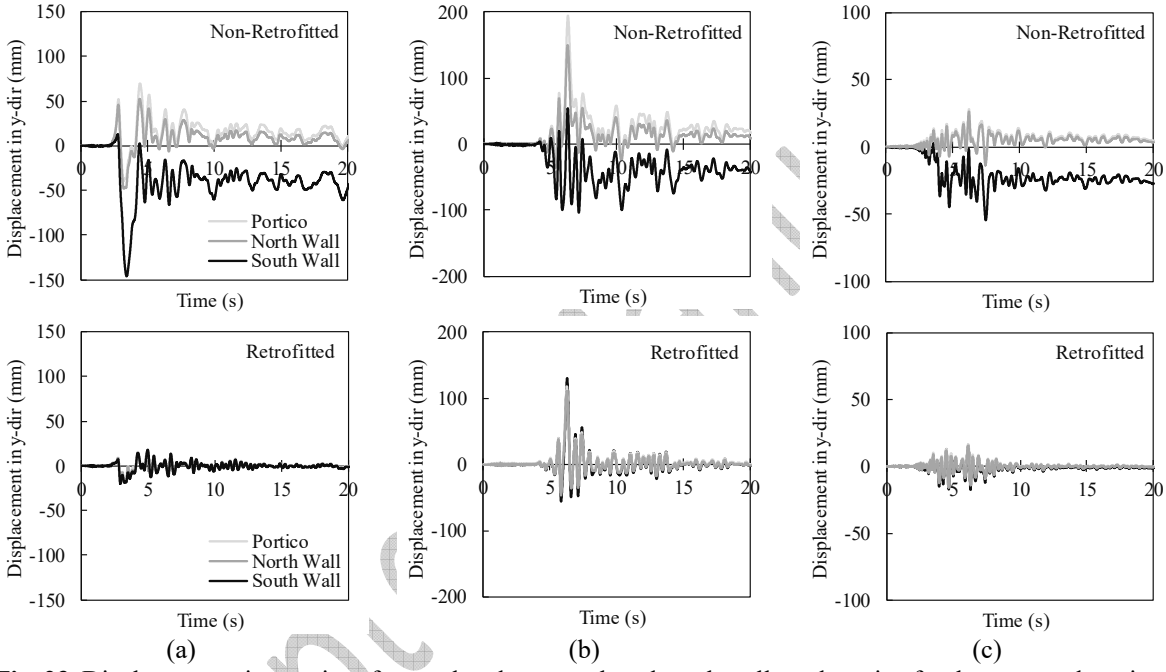

Fig. 23. Displacement-time series of control nodes at north and south walls and portico for three ground motions in y-direction, (a) Erzincan, (b) Düzce – Bolu, (c) Bingöl

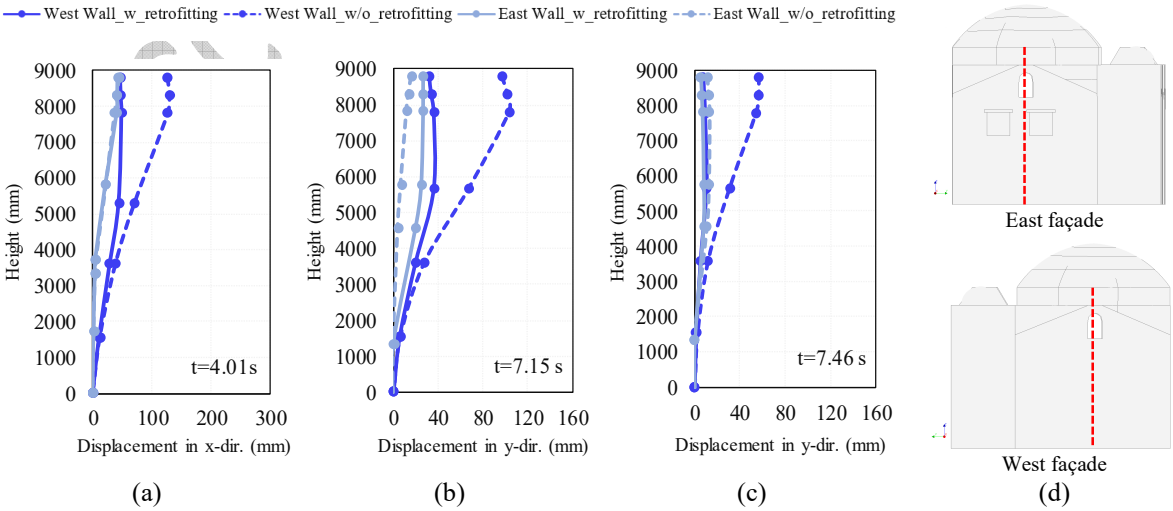

Fig. 24. Change in out-of-plane behavior in terms of absolute displacement at time-step when west wall has peak displacement, (a) Erzincan, (b) Düzce - Bolu, (c) Bingöl, (d) location of the section cuts

5.2.2 Change in relative out-of-plane displacement at the dome supporting walls

The retrofitting action was conducted to provide a global structural behavior to the structure by improving the connection between contiguous structural elements. The dome experiences expansion if the interaction between its support, i.e. load-bearing walls and drum, is not provided. A schematic representation of the dome expansion is given in Fig. 25 by considering the west and east walls (transverse direction). In the non-retrofitted model, different displacements are expected on each parallel wall due to the lack of global structural behavior, and, therefore higher relative displacements can be observed (Fig. 25(b)). Relative displacements of the walls were investigated in terms of residual displacements due to the observed response in the non-retrofitted case. Once the retrofitted model achieves box behavior, lower relative residual displacements are expected comparing to the former case. Providing that $\Delta res_2 << \Delta res_1$, limited damage is expected in the retrofitted case (Fig. 25(c)). Within this context, the relative out-of-plane movement of the adopted control nodes on the dome supporting walls were calculated and presented only for transversal direction with respect to the west wall (Fig. 26).

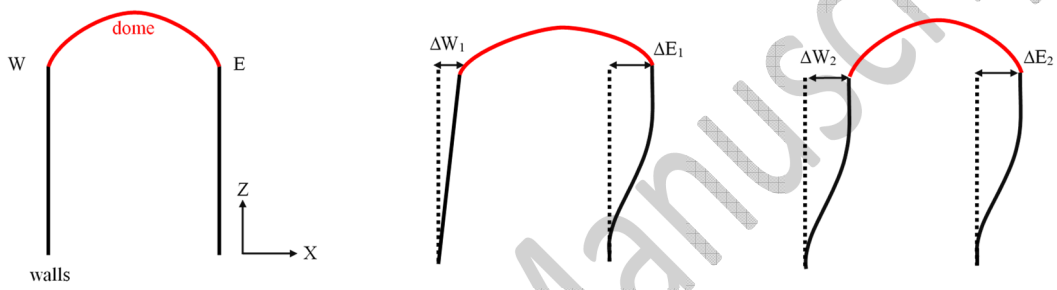

Fig. 25. Schematic representation of the residual displacements on the dome supporting walls

Additionally, relative residual displacements were computed by taking the average of the displacement in the time interval after the ground motion reaches nearly 90% energy, which corresponds to 10 s to 20 s of each record in Fig. 22. Relative out-of-plane displacement in the non-retrofitted model is high, which leads to expansion of the dome and results in high tensile stresses. As stated before, severe damage in the form of large cracks was observed on the dome during the site investigations. It can be concluded that the high relative displacements in the out-of-plane directions contributed to the severe cracks observed on the dome. On the contrary, an improvement in the response for the retrofitted model is clear and is presented in Fig. 27 for both directions. A limited expansion of the dome in both orthogonal directions can be addressed due to presence of steel girders.

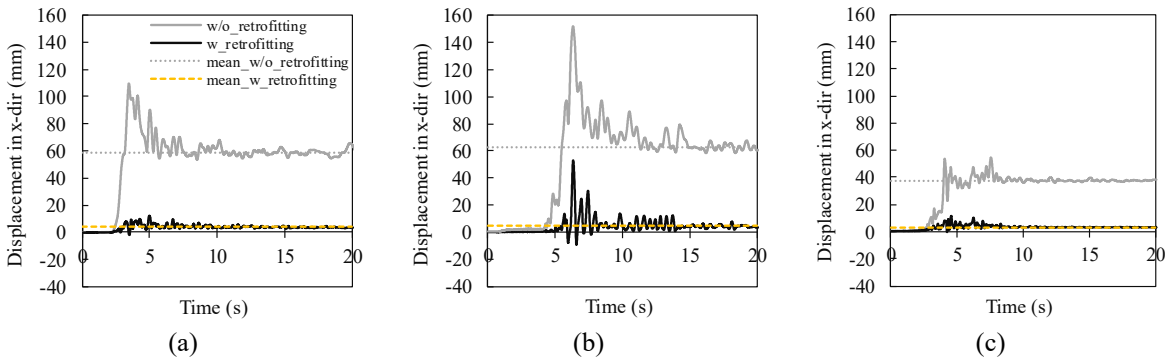

Fig. 26. Change in out-of-plane displacement relative to the west wall, (a) Erzincan, (b) Düzce – Bolu, (c) Bingöl

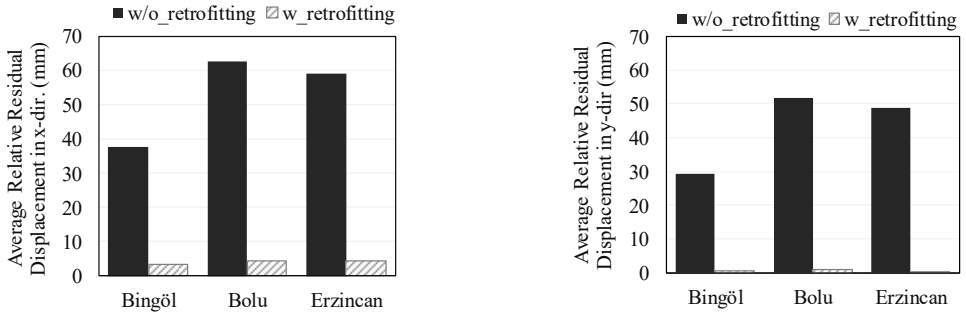

Fig. 27. Variation in the average relative residual displacement with respect to each ground motion, (a) transversal direction, (b) longitudinal direction

5.2.3 Change in the absolute acceleration response

Absolute acceleration is another important engineering parameter in terms of seismic forces acting on structural and non-structural components. Historical masonry buildings are very stiff and respond with high spectral accelerations. Serviceability of the masonry components should be satisfied, often including artistic decoration (movable, such as paintings or structures, or immovable, such as frescoes). The absolute acceleration response on non-retrofitted and retrofitted model was computed at the highest point of the numerical model, i.e. the top point of the dome. Acceleration-time series on the control point are given for the non-retrofitted and retrofitted Mosque in transversal direction (Fig. 28). For the longitudinal direction, similar values are obtained (maximum of 0.85g for retrofitted model vs. 0.55g for non-retrofitted model). Increased absolute acceleration values were observed due to steel girder retrofitting in both directions. It can be inferred from the absolute acceleration-time series that, with the achievement of global structural behavior, so-called box behavior, by means of the applied retrofitting scheme, the absolute acceleration response at the dome is increased. This will certainly increase the inertial forces imposed on the dome, meaning that retrofitting may have detrimental effects, particularly to movable artistic decorations.

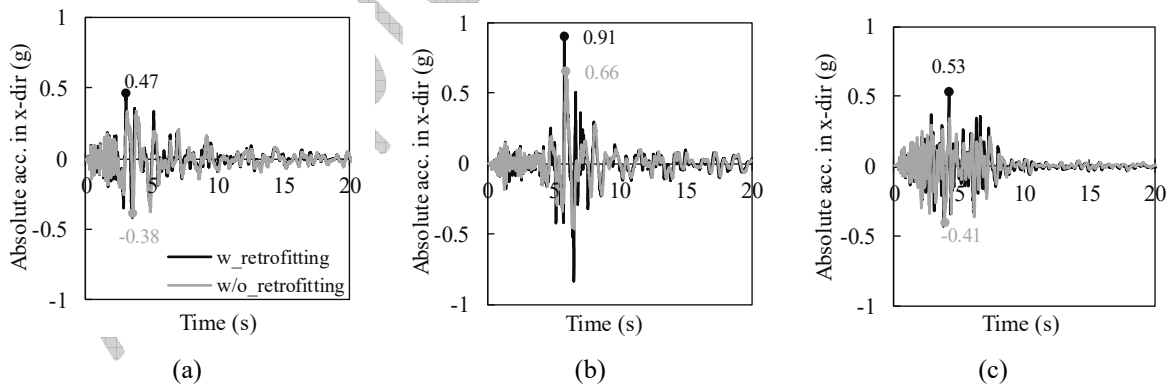

Fig. 28. Change in absolute acceleration response in transversal direction, (a) Erzincan, (b) Düzce – Bolu, (c) Bingöl

5.2.4 Correlation of the cracks and change in response in terms of principal tensile strain distribution

Principal tensile strains were plotted for the time-step when each numerical model had its own critical condition. At the time-step when the control point reached the peak displacement on each structural component, the principal tensile strain distribution of the global structure was examined, and the most critical plot (with largest strain) was selected for each case. The existing cracks on the Mosque were satisfactorily reproduced—for instance, as seen in

Fig. 29, Fig. 30, and Fig. 31—the strain distribution on the south, west, and east façades presented similar damage pattern to Fig. 17, respectively, when numerical model subjected to different dynamic loadings. In fact, the strain pattern obtained from the retrofitted case shows that the structure was dominated by in-plane behavior, whereas out-of-plane movement was observed in the non-retrofitted case (see Fig. 29).

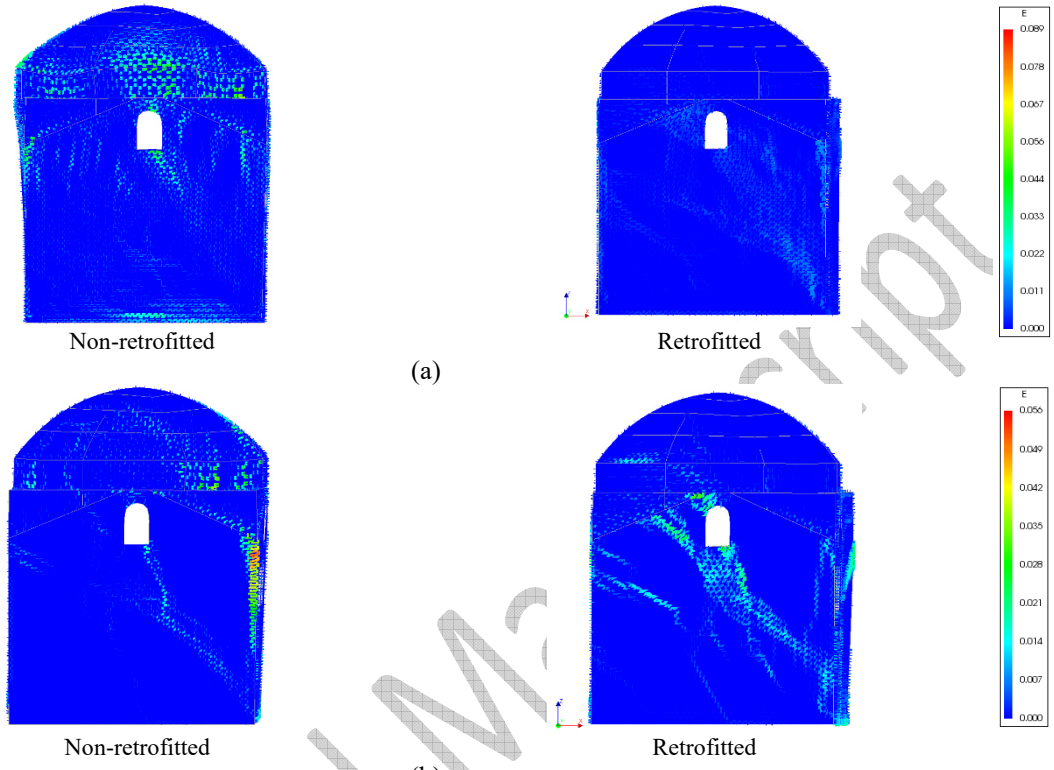

Fig. 29. Total principal tensile strain distribution on the south façade of the numerical models due to dynamic loading, (a) Erzincan Earthquake at time-step 3.43s, (b) Bingöl Earthquake at time-step 3.99s

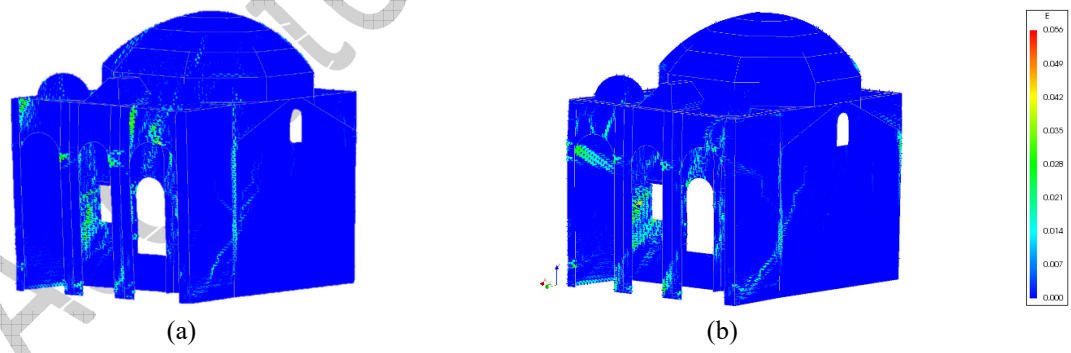

Fig. 30. Total principal tensile strain distribution on the west façade of the numerical models subjected to the Bingöl Earthquake, at time-step 3.99s, (a) non-retrofitted, (b) retrofitted

Moreover, nonlinear dynamic analyses satisfactorily reproduce the damage observed on the dome, in which the orientation of the parallel cracks shown in Fig. 3 and Fig. 4 are compatible with the principal tensile strain distribution (Fig. 32). Fig. 3 illustrates that both parallel cracks propagate until the drum section, which was also observed on the non-retrofitted numerical model, and the concentration of the tensile strains corresponds to the location of the real damage.

Based on the conducted comparisons, the correlation of the in-situ investigations and dynamic analyses results are compatible. Numerical cases are in a good agreement with the real damage and several conclusions could be made; the non-retrofitted structure is dominantly subjected to out-of-plane behavior, which results high tensile stresses on the significant portion of the structure. Still, even with the retrofitting, the structure experiences damage under dynamic loading. However, it is important to mention that the out-of-plane movement of the retrofitted structure walls is limited considerably. In case of the overall nonlinear response is originated by in-plane behavior, which constitutes the desired type of behavior, higher energy dissipation can occur by avoiding the total collapse, as emphasized by Magenes and Calvi (1997). Therefore, effectiveness of the applied retrofitting scheme can be concluded within the scope of the case study.

(a) (b)

Fig. 31. Total principal tensile strain distribution on the east façade of the numerical models subjected to the Bingöl Earthquake, at time-step 3.99s, (a) non-retrofitted, (b) retrofitted

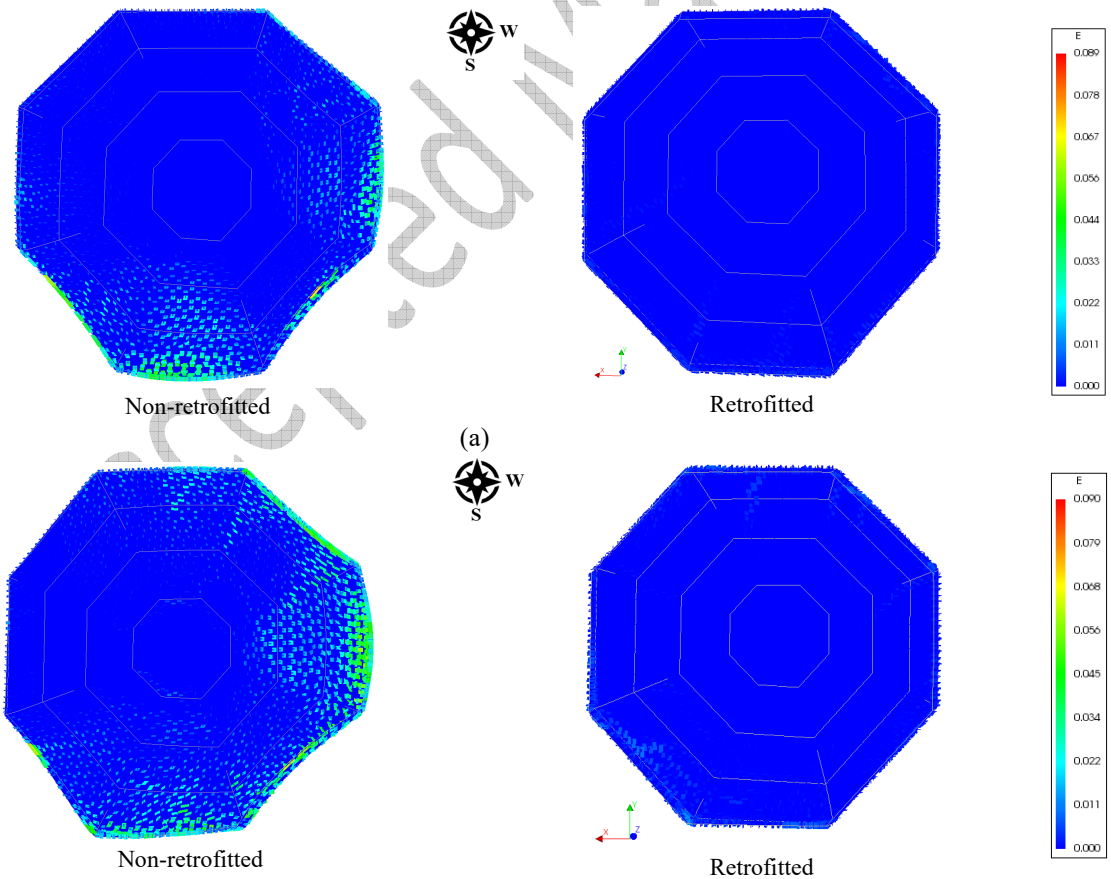

Fig. 32. Total principal tensile strain distribution on the dome of the numerical models subjected to (a) the Erzincan Earthquake at time-step 3.43s, (b) the Bolu Earthquake at time-step 6.12s

At last, it is important to notice that the vertical components of the earthquakes were disregarded in the numerical model due to numerical convenience reasons. This is still an open issue, as observed in the current guidelines as TEC 2007, the EC8 and NTC2008, which allow to ignore its effect on the ground motion adopted for the analysis. The selected earthquakes have a lower vertical PGA with respect to the associated horizontal ones, which does not guarantee, by itself, that its effect in the response is not significant. In fact, it should be highlighted that these may have an implication in the structural behavior of the Mosque, by lessening the pre-compression levels and, therefore, increase the possibility of shear-induced mechanisms to occur easily (Papazoglou and Elnashai, 1996). Even so, a test has been performed using the Bolu record which is the case where the most unfavorable results have been obtained. The results show that, if the vertical component was active, an insignificant difference of 1.8% was found for the horizontal displacements. Conversely, a difference around 15% was found for the vertical displacement of the control node located in the dome pinnacle (Node 1). Still, the damage pattern does not show a significant difference, which supports the decision of not including the vertical seismic component.

6 Summary and Conclusions

This paper addressed the seismic assessment of the Kütahya Kurşunlu Mosque, located in the Turkey seismic-prone province of Kütahya. Being part of the country's architectural heritage, the Directorate General of Foundations of Turkey ordered, in 2013, the application of restoration works and seismic retrofitting actions over the Mosque. The retrofitting interventions, based on the application of steel girders, aimed to provide a better interaction between the different structural subparts of the Mosque and, therefore, to decrease the associated seismic vulnerability.

The Mosque was subjected to three high intensity earthquakes occurred in March 1970, April 1970, and in May 2011 which, combined with past long-term effects on the structure, enforced both the study over the current condition and over the effectiveness of the retrofitting technique adopted. The primary aim is to ensure safety for future events. A scientific-based procedure has been followed, which encompasses visual inspections, ambient dynamic identification tests, and the development of two numerical FE-based models. The visual inspections are crucial for a better understanding of the geometrical features of the structure and to survey the existing damage. Regarding the dynamic identification tests, the obtained data allowed to perform the elastic calibration of the numerical model (fitting the Young's modulus of masonry) through eigenvalue analyses. The numerical models based on a macroscopic FE-modelling approach allowed to assess the seismic response of both the retrofitted and non-retrofitted structure. It may be remarked that no experimental campaign was undertaken to determine the strength and nonlinear properties of the masonry, and, therefore, these values were defined according to the existing literature. Given the uncertainties, even if the conclusions on the seismic capacity are not necessarily absolutely correct, the analyses are still useful and valid for relative comparison terms.

Quasi-static (pushover) and dynamic analyses (accounting with the three real earthquakes that occurred in Turkey) were performed and allowed to point out some conclusions:

- Although the steel retrofitting elements seem to not influence the elastic behavior of the structure, it appears to affect its nonlinear response—in particular, the behavior of load-bearing walls;
- The pushover analyses showed that the lateral envelope capacity of both the retrofitted and non-retrofitted models is higher for the y-direction (longitudinal direction);
- Increased absolute acceleration values were observed due to the steel girder retrofitting in both directions, around 28% and 35% for the x- and y-directions, respectively;

- The retrofitting scheme allowed to clearly increase the ductility of the structure for both the x- and y-directions. It tried to avoid the out-of-plane mechanisms and enforced the formation of in-plane mechanisms to occur with more capacity to dissipate energy. A decrease of the relative out-of-plane deformation between the east and west façades was also found, which contains the opening of existing cracks and the expansion of the dome.

Generally, the numerical damage seems in good agreement with the data collected from the in-situ damage survey, and, despite the different character between static and dynamic lateral loading, both exhibited similar failure modes. Note that numerical damage was analyzed by plotting the obtained principal strains distribution, which seems to be a good and convenient indicator, as found in other works in the literature, when using a macro-modelling FE-based approach. On the other hand, such a modelling approach proved to be adequate in reproducing the actual response of the Mosque, and, therefore, it constitutes a good option for the study of such large structures, bearing in mind the existing trade-off between the results accuracy and computational cost.

At last, the authors would like to stress that, based on the absolute acceleration response obtained at the top of the dome, the seismic retrofitting imposed higher acceleration to the structure. This can be an indication of a stiffer structural system for the dome by means of the global behavior (so-called box type of behavior), which may have detrimental effect in artistic assets, particularly the movable ones. Thus, it is highlighted that the acceleration response should be also part of the concern when planning a seismic assessment analysis and retrofitting intervention on this type of structure.

Acknowledgements

The authors thank Dr. Onur Kaplan, research assistant at Eskişehir Technical University, for his experimental campaign for the ambient vibration measurements of the Kütahya Kurşunlu Mosque and Georgios Karanikoloudis, PhD student at University of Minho, for the knowledge shared to perform operational modal analysis.

References

AFAD (2018) Earthquake Hazard Map of Turkey

Aguilar R, Torrealva D, Ramos LF, Lourenço PB (2012) Operational Modal Analysis Tests on Peruvian Historical Buildings : The Case Study of the 19 th Century Hotel Comercio. In: 15th World Conference on Earthquake Engineering, Lisbon Portugal

Almac U, Alaboz M, Bal IE, et al (2016) Structural observations on Macedonian tower, Edirne. Struct Anal Hist Constr Anamn diagnosis, Ther Control - Proc 10th Int Conf Struct Anal Hist Constr SAHC 2016 1764–1768

Angelillo M, Lourenço P, Milani G (2014) Masonry behavior and modelling. In: Angelillo M (ed) Mechanics of Masonry Structures. CISM International Centre for Mechanical Sciences, Springer, Udine, pp 1–24

ARTeMIS Modal SVS-Structural Vibration Solutions A/S

Braga AAB (2014) Study of the Armenian Church in Famagusta. University of Minho

CEB-FIP (1993) Model Code 90. Thomas Telford Ltd, UK

Ciocci MP, Sharma S, Lourenço PB (2018) Engineering simulations of a super-complex cultural heritage building: Ica Cathedral in Peru. Meccanica 53:1931–1958. doi: 10.1007/s11012-017-0720-3

EC8 CEN, 2005. EN 1998-3 - Eurocode 8: Design of structures for earthquake resistancepart 3: Assessment and retrofitting of buildings

FX+ for DIANA (2013) Midas FX+ for DIANA, Customized Pre/Post-processor for DIANA

Gentile C, Saisi A (2007) Ambient vibration testing of historic masonry towers for structural identification and damage assessment. Constr Build Mater 21:1311–1321

ICOMOS (2013) ICOMOS Turkey Architectural Heritage Conservation Charter

Italian Code C (2009) Technical Standards for Constructions - DM 14/01/2008. In: Gazzetta Ufficiale Serie Generale n.47 del 26/02/2009. Italy

Kalkan E, Gülkan P (2004) Site-dependent spectra derived from ground motion records in Turkey. Earthq Spectra 20:1111–1138. doi: 10.1193/1.1812555

Karanikoloudis G, Lourenço PB (2018) Structural assessment and seismic vulnerability of earthen historic structures. Application of sophisticated numerical and simple analytical models. Eng Struct 160:488–509. doi: https://doi.org/10.1016/j.engstruct.2017.12.023

Kazaz İ, Kocaman İ (2018) Seismic load capacity evaluation of stone masonry mosques. J Fac Eng Archit Gazi Univ. doi: 10.17341/GUMMFD.30784

Kocaman İ, Kazaz İ, Okuyucu D (2018) Tarihi Erzurum Yakutiye Medresesi'nin Yapısal Davranışının İncelenmesi. Dokuz Eylul Univ J Sci Eng 20:. doi: 10.21205/deufmd.

KOERI Boğaziçi University Kandilli Observatory and Earthquake Research Institute Regional Earthquake-Tsunami Monitoring Center

Lara R (2016) Structural analysis of the church of the Monastery of São Miguel de Refojos. University of Minho

Lourenço, Krakowiak KJ, Fernandes FM, Ramos LF (2007) Failure analysis of Monastery of Jerónimos, Lisbon: How to learn from sophisticated numerical models. Eng Fail Anal 14:280–300. doi: 10.1016/j.engfailanal.2006.02.002

Lourenço PB (2002) Computations on historic masonry structures. Prog Struct Eng Mater 4:301–319. doi: 10.1002/pse.120

Lourenço PB, Mendes N, Ramos LF, Oliveira D V. (2011) Analysis of Masonry Structures Without Box Behavior. Int J Archit Herit 5:369–382. doi: 10.1080/15583058.2010.528824

Lourenço PB, Trujillo A, Mendes N, Ramos LF (2012) Seismic performance of the St. George of the Latins church: Lessons learned from studying masonry ruins. Eng Struct 40:501–518. doi: 10.1016/j.engstruct.2012.03.003

Magenes G, Calvi GM (1997) In-plane seismic response of brick masonry walls. Earthq Eng Struct Dyn 26:1091–1112. doi: 10.1002/(SICI)1096-9845(199711)26:11<1091::AID-EQE693>3.0.CO;2-6

Mangia L, Ghiassi B, Sayın E, et al (2016) Pushover Analysis of Historical Eltihatun Mosque. In: 12th International Congress on Advances in Civil Engineering. İstanbul

Mendes N (2012) Seismic Assessment of Ancient Masonry Buildings : Shaking Table Tests and Numerical Analysis. University of Minho

Nohutcu H, Demir A, Ercan E, et al (2015) Investigation of a historic masonry structure by numerical and operational modal analyses. Struct Des Tall Spec Build 821–834

NTC2008 Italian Code for Structural Design (Norme tecniche per le costruzioni - NTC). D.M. 14/01/2008, Official Bullettin no. 29 of February 4th, 2008, In Italian

Orbaşlı A (2007) Architectural Conservation: Principles and Practice. Wiley-Blackwell

Ozturk B (2017) Seismic behavior of two monumental buildings in historical Cappadocia region of Turkey. Bull Earthq Eng 15:3103–3123. doi: 10.1007/s10518-016-0082-6

P. Roca (2006) The study and restoration of historical structures: From principles to practice. In: P.B. Lourenço, P. Roca, C. Modena SA (ed) Structural analysis of historical constructions. pp 9–24

Papazoglou AJ, Elnashai AS (1998) Analytical and field evidence of the damage effect of vertical earthquake ground motion. Earthq Eng Struct Dyn 25:1109–1137. doi: 10.1002/(SICI)1096-9845(199610)25:10<1109::AID-EQE604>3.0.CO;2-0

Ramos LF, Aguilar R, Lourenço PB (2010a) Operational modal analysis of historical constructions using commercial wireless platforms. Struct Heal Monit 10:511–521

Ramos LF, Marques L, Lourenço PB, et al (2010b) Monitoring historical masonry structures with operational modal analysis : Two case studies. Mech Syst Signal Process 24:1291–1305

Sevim B, Bayraktar A, Altunişik AC, et al (2011) Assessment of nonlinear seismic performance of a restored historical arch bridge using ambient vibrations. Nonlinear Dyn 63:755–770

Silva LC, Mendes N, Lourenço PB, Ingham J (2018) Seismic Structural Assessment of the Christchurch Catholic Basilica, New Zealand. Structures 15:115–130. doi: https://doi.org/10.1016/j.istruc.2018.06.004

TEC (2007) Turkish Earthquake Code: Specifications for the Buildings to be Constructured in Disaster Areas. In: Official Gazette No 26454. Ankara

TNO DIANA (2017) User's Manual Release 10.2

Tomaževič M (1999) Earthquake-Resistant Design of Masonry Building. Imperial College Press, London

TR-NSMN Strong Motion Database. In: AFAD

Trifunac MD, Brady AG (1975) A study on the duration of strong earthquake ground motion. Bull Seismol Soc Am 65:581–626

Valente M, Milani G (2018) Seismic Response Evaluation and Strengthening Intervention of Two Historical Masonry Churches. In: Milani G, Taliercio A, Garrity S (eds) 10th International Masonry Conference. Milan

Yılmaz N, Avşar Ö (2013) Structural damages of the May 19, 2011, Kütahya-Simav earthquake in Turkey. Nat Hazards 69:981–1001. doi: 10.1007/s11069-013-0747-2